

Research



Cite this article: West BJ, Culbreth G, Dunbar RIM, Grigolini P. 2023 Fractal structure of human and primate social networks optimizes information flow. *Proc. R. Soc. A* **479**: 20230028.
<https://doi.org/10.1098/rspa.2023.0028>

Received: 12 January 2023

Accepted: 3 May 2023

Subject Areas:

statistical physics, fractals

Keywords:

networks, Dunbar's number, attractors, criticality, information, collective intelligence

Author for correspondence:

Robin I. M. Dunbar

e-mail: robin.dunbar@psy.ox.ac.uk

Fractal structure of human and primate social networks optimizes information flow

Bruce J. West¹, Garland Culbreth¹, Robin I. M.

Dunbar² and Paolo Grigolini¹

¹Center for Nonlinear Science, University of North Texas, Denton, TX 76203, USA

²Department of Experimental Psychology, University of Oxford, Radcliffe Observatory Quarter, Oxford OX2 6GG, UK

RIMD, 0000-0002-9982-9702

Primate and human social groups exhibit a fractal structure that has a very limited range of preferred layer sizes, with groups of 5, 15, 50 and (in humans) 150 and 500 predominating. In non-human primates, this same fractal distribution is also observed in the distribution of species mean group sizes and in the internal network structure of their groups. Here we demonstrate that this preferential numbering arises because of the critical nature of dynamic self-organization within complex social networks. We calculate the size dependence of the scaling properties of complex social network models and argue that this aggregate behaviour exhibits a form of collective intelligence. Direct calculation establishes that the complexity of social networks as measured by their scaling behaviour is non-monotonic, peaking globally around 150 with a secondary peak at 500 and tertiary peaks at 5, 15 and 50. This provides a theory-based rationale for the fractal layering of primate and human social groups.

1. Introduction

Human personal social networks have a characteristic size (approx. 150) with a distinctive layered structure based on a hierarchically inclusive series of layers at 5, 15 and 50 within the 150 and then continuing as an external series of layers at 500 and 1500 [1].

© 2023 The Authors. Published by the Royal Society under the terms of the Creative Commons Attribution License <http://creativecommons.org/licenses/by/4.0/>, which permits unrestricted use, provided the original author and source are credited.

Counting cumulatively, these layers have a very consistent scaling ratio of approximately 3 across a range of contexts including (but not limited to) ego-centric social networks [2], online social networks [3,4], cellphone communication networks [4,5] and even trading networks in stock exchanges [5]. The same motif appears in the structural organization of hunter–gatherer societies [6], the design of leisure facilities such as caravan parks [7], the size and structure of alliances in online gaming environments [8] and the structural organization of modern armies [9]. Moreover, the same pattern has been noted in the distribution of group sizes across primate species [10], as well as in the internal structuring of primate social groups [11,12].

The fact that this pattern seems to be so widespread in so many different social contexts suggests that it is underpinned by very general structural principles. It has been noted that social group size in primates is correlated with brain size [13,14], and that this correlates in turn with environmental threats such as predation risk [14,15]. Despite these empirical relationships, it has proven difficult to find any convincing first principles explanations that might explain why social groupings across both humans and primates have the particular structure they do, and why they should form such a specific fractal pattern.

West *et al.* [16] provide a *prima facie* case for the viewing efficiency of information flow through networks as being crucial for the structural stability of natural human social groups (equivalent to the 150 layer). They used two different models of group social dynamics (a decision-making model (DMM) and a swarm intelligence model (SIM)) to generate criticality-induced intelligence as a function of social group size. This analysis established computationally that the scaling of the network time series varies non-monotonically with network size. In the DMM, N individuals choose between two conflicting decisions under the influence of their neighbours [17]; in the SIM, the behaviour of a group (such as the response of a flock of birds in flight from a predator) is determined by the binary choice between continuing on-course or changing course to escape [18]. These models are derivative of a class of Ising models widely used in the study of opinion dynamics (i.e. the flow of information through networks), social physics and complexity science [9,19–21]. All these models assume that spatial or social adjacency results in neighbours converging on a common opinion or behaviour through copying, infection or some form of cultural transmission. As such, they apply to a wide variety of social and other contexts.

In both DMM and SIM models, criticality is identified as a condition for optimum information flow in complex networks. Both models turn out to have criticality in their dynamics [16], with the second moment of the global time series from these models scaling as a power law in time $t^{2\delta}$. The scaling index δ has an optimum value of approximately $2/3$, peaking globally at the Dunbar Number $N = 150$ and falling steeply away on either side of this value. The dependence of the scaling index on network size is one signature of complexity and the calculations in West *et al.* [16] establish that networks of size $N = 150$ have optimal information transmission properties, in agreement with the principle of complexity matching (PCM) [22]. The time interval τ between consecutive ‘crucial events’ (CEs, or state change events) is given by the waiting-time probability density function (PDF) $\psi(\tau)$, sharing in the intermediate asymptotic regime [23] with the same inverse power law (IPL) structure as the hyperbolic PDF

$$\psi(\tau) = (\mu - 1) \frac{T^{\mu-1}}{(T + \tau)^\mu} \quad (1.1)$$

with $1 < \mu < 3$. The PCM has been experimentally observed in the information exchange that occurs between complex networks in a substantial number of naturally occurring interactions, including turn taking in dyadic conversation [24], the therapeutic influence of arm-in-arm walking [25] and the influence of zealots on group behaviour [17]. Following West *et al.* [17], the tools of network science can then be used to explore the way information flows within and between these networks in order to identify network sizes where the efficiency of information flow is optimized.

We here extend this approach and ask whether, in addition to the principal layer at 150 identified by West *et al.* [16], the other layers that have been identified in human and primate

social networks [1] are also local maxima. In other words, given that the Dunbar Number of approximately 150 has been shown to be the result of dynamic criticality in terms of the efficiency with which information flows through social networks [16], we use this same approach to test the hypothesis that the layers that immediately surround this value in human social groupings (i.e. network layer sizes of 5, 15, 50 and 500) are local dynamic criticalities that represent harmonics of the Dunbar Number. If so, we may then be able to provide a first principles theoretical explanation for the network sizes that appear in both the distribution of group sizes and the fractal layering of social networks within groups—not just in humans, but also in primates.

Note that we use ‘information’ here in the cybernetic sense introduced by Wiener [26]. In this sense, it can refer to anything that constitutes a tie or attraction between nodes in a network. Hence, while we phrase our analysis in terms of ‘information flow’ between nodes, this might be actual information (passed on by cultural transmission, learning or teaching) or it might be the ‘gravitational’ attraction between social partners [27] created in primates by social grooming or in humans by activities like conversation, laughter or storytelling [28]. This same generic usage has been used to underpin models of economic Webs in global finance and stock markets, the social meshes of governments and terrorist organizations, the transportation networks of planes and highways, the eco-Webs of food networks and species diversity, the physical wicker of the Internet and the bio-net of gene regulation.

2. Methods

Following West *et al.* [16], we consider a conventional opinion dynamics (or swarm intelligence) Ising-type diffusion model where N individuals (nodes) are mapped onto an $N \times N$ array. Each node is assigned an initial status synonymous with a compass direction. In successive iterations, each node can alter its status following interaction with adjacent nodes, as a result of which nodes, and the network as a whole, can switch in and out of synchrony.

We begin by relating complexity to the use of scaling theory in the search for the origin of an anomalous series $\xi(t)$ and then use a mobile window to transform the fluctuations characterized by $\xi(t)$ into many diffusional trajectories $X(t)$. Stanley *et al.* [29,30] introduced this technique by treating DNA sequences as steps in a simple random walk (RW) process. The purpose of the RW procedure was to establish that the departure of $\xi(t)$ from a completely random function could be detected through the departure of the scaling of $X(t)$ from ordinary diffusion by means of a scaling index δ different from the default baseline of $\delta = 0.5$. We extend this technique by interpreting $X(t)$ as being the carrier of CEs that may be different from those hosted by $\xi(t)$. In other words, we interpret $X(t)$ as being a time series, which can be analysed by studying its diffusive properties. If the subsequent diffusion is anomalous, we adopt the nomenclature from the sociology literature and view the subsequent dynamics as a form of SIM [31].

In the case of the SIM, the fluctuations $\xi(t)$ denote the fluctuating velocity of a swarm. It is important to stress that to detect the action of CEs, in which the time intervals between consecutive events are renewed with IPL statistics having an index μ , we convert the fluctuations $\xi(t)$ into a diffusion process. For each of the N members of the swarm, the time step is taken for convenience to be $\Delta t = 1$, and the position at each successive time step is calculated using:

$$X_j(t+1) = X_j(t) + V_j(t)\Delta t, \quad (2.1)$$

with the unit's velocity given by a magnitude $|V|$ and angle θ . The direction of the unit j is given by

$$\theta_j(t+1) = \langle \theta_j(t) \rangle_r + \Delta \theta_j, \quad (2.2)$$

where $\langle \theta_j(t) \rangle_r$ is the average direction of all units within a circle of radius r , at time t of unit j and $\Delta \theta_j$ is a random number chosen from the interval $[-1.75, 1.75]$. For every simulation, the range of the random variable was the same and the constant speed had the magnitude $|V| = 0.05$.

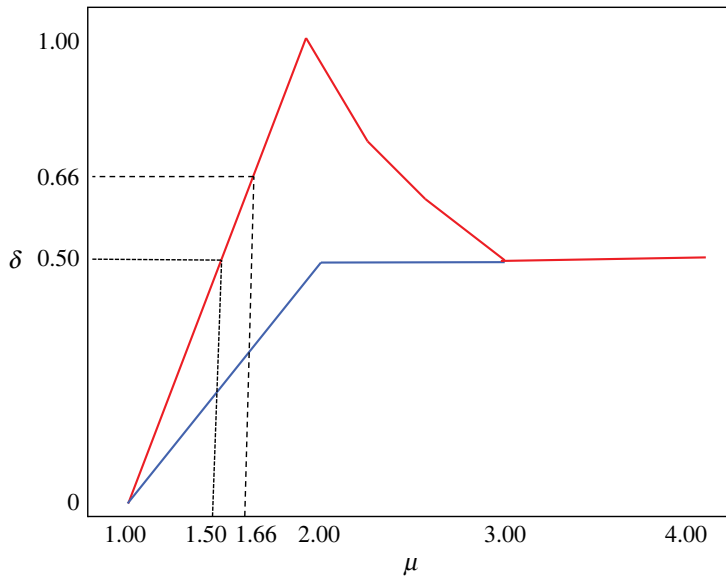


Figure 1. The relationships between the diffusional scaling index δ and the crucial event index μ are depicted. The blue line corresponds to constraining the steps in DEA to always be positive. For this case: $1 < \mu < 2$, $\delta = (\mu - 1)/2$. The red line corresponds to the case where this constraint is not adopted. For that case: $1 < \mu < 2$, $\delta = \mu - 1$; $2 < \mu < 3$, $\delta = 1/(\mu - 1)$. Herein we observe values of δ in the range $0.5 \leq \delta \leq 0.667$, and values μ corresponding to them. From the study of West *et al.* [33] with permission.

The mean global field at each time step is calculated, following [18], as

$$\xi(t) = \frac{1}{N|V|} \left| \sum_{n=1}^N \lceil V \rceil e^{i\theta_n(t)} \right|, \quad (2.3)$$

and the resulting diffusion process is

$$X(t) = X(0) + \int_0^t \xi(t') dt'. \quad (2.4)$$

A statistical analysis of time series generated by network models of criticality-induced intelligence can then be run on the diffusion process generated by equation (2.4) for a wide range of network sizes in order to detect CEs using diffusion entropy analysis (DEA) [32]. In the sections that follow, we describe the procedure for doing so.

(a) Method of stripes

We use the diffusion process generated by equation (2.4) to evaluate the scaling index δ . In the fluctuating mean field $\xi(t)$, each fluctuation corresponding to a CE is either positive or negative and the scaling is given by $\delta = (\mu - 1)/2$ for $\mu < 2$ and by $\delta = 1/2$ for $\mu > 2$. This is described by the blue curve in figure 1. However, West *et al.* [33] showed that converting the negative fluctuations into positive fluctuations has the effect of making the detection of the scaling index δ much more accurate. This changing of negative to positive fluctuations corresponds to moving from the blue to the red curve in figure 1. It is important to stress that the results discussed herein show that the networks at criticality move from the condition $\delta = 1/2$ generated by CEs with IPL index $\mu = 3/2$ to $\delta = 2/3$ where the opinion-persistence manifests a scaling index identical to the power law index of the CEs [33].

Following West *et al.* [33], the diffusion trajectory $X(t)$ used for the scaling evaluation is built up by forcing the random walker to make a jump ahead of constant intensity when a fluctuation

occurs. An alternative but equivalent approach rests on the fluctuations $\xi(t)$ generated by SIM. Using the method of the stripes (MoS), we record the times at which the fluctuations $\xi(t)$ cross the border between two consecutive stripes. Should these events not be crucial, they would not contribute to the scaling emerging in the long-time limit. Furthermore, when an event occurs, the random walker always makes a step ahead of constant intensity (length). The observation of the fluctuations ξ in equation (2.3) does not require the adoption of stripes but only needs the negative values of ξ to be converted into positive values.

(b) Diffusion entropy analysis

Once the diffusional trajectory is properly created based on CEs, we can use a mobile window of size l to explore the whole diffusional trajectory of length l . For any window position, we record the difference between $X(t)$ at the end of the window and $X(t)$ at the beginning of the window, interpreting this as a time-interval travelled by a random walker in the time interval l . Due to the large number of window positions, we can define the PDF $p(x, l)$ and the Shannon/Wiener entropy $S(l)$:

$$S(l) = - \int_{-\infty}^{\infty} p(x, l) \log_2[p(x, l)] dx. \quad (2.5)$$

Under the assumption that the above diffusion process yields the scaling structure determined by the CEs, the PDF has the scaling form:

$$p(x, l) = \frac{1}{l^\delta} F\left(\frac{x}{l^\delta}\right), \quad (2.6)$$

which when inserted into equation (2.5) yields:

$$S(l) = A + \delta \log_2(l), \quad (2.7)$$

where A is a constant determined by the unknown function $F(\cdot)$. This reasoning enables us to interpret the slope of the curve generated by graphing $S(l)$ versus $\log_2(l)$ as the scaling index δ of the diffusion process.

(c) Modified diffusion entropy analysis

In the present case, we use the *modified diffusion entropy analysis* (MDEA) procedure developed by West *et al.* [16] because it is especially suited for determining the existence of anomalies in the scaling of diffusion processes. When swarm or criticality-induced intelligence [31] becomes active, the constructed process is expected to depart from ordinary diffusion as measured by a scaling index different from $\delta=0.5$. Culbreth *et al.* [32] noted that the original version of DEA cannot assess whether the deviation from the scaling $\delta=0.5$ is due to the action of CEs or the infinite memory contained in *fractional Brownian motion* (FBM) [34]. By contrast, the MDEA procedure filters out the scaling behaviour of infinite stationary memory of FBM, when it exists, and the remaining departure of the scaling index from $\delta=0.5$ is then solely a consequence of CEs.

It is important to notice that in the DEA the diffusion trajectory $X(t)$ is realized using the experimental data $\xi(t)$ directly. In the more refined version using the MoS given by Culbreth *et al.* [32], we obtain the MDEA. Figure 2 shows the result of this procedure in the case where MDEA is used with the stochastic equation (2.4). Similar results are obtained by using the detection of CEs through the stripes. It is important to stress that the adoption of MDEA makes $S(l)$ a linear function of $\ln(l)$ in an extended time l interval. We refer to this scaling domain as the intermediate asymptotic region. At small values of l , the IPL index of the CEs μ is not yet perceived. In the long-time l region, the deviation from the linear behaviour is usually due to the small number of CEs and consequently to statistical inaccuracy.

The MDEA method applied to the signal $X(t)$ generated by the criticality-induced intelligence time-series driving the rate equation $(dX(t)/dt) = \xi(t)$ implements the original DEA in conjunction

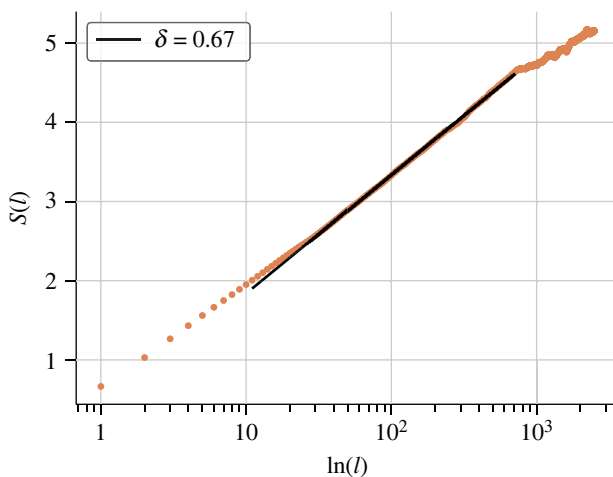


Figure 2. The Shannon/Wiener entropies (orange dots) at each window length l , measured by MDEA on time-series data generated by the SIM mean field for 150- and 10 000-time steps. The scaling is the slope of the linear portion and gives $\delta = 0.67$ (solid black line).

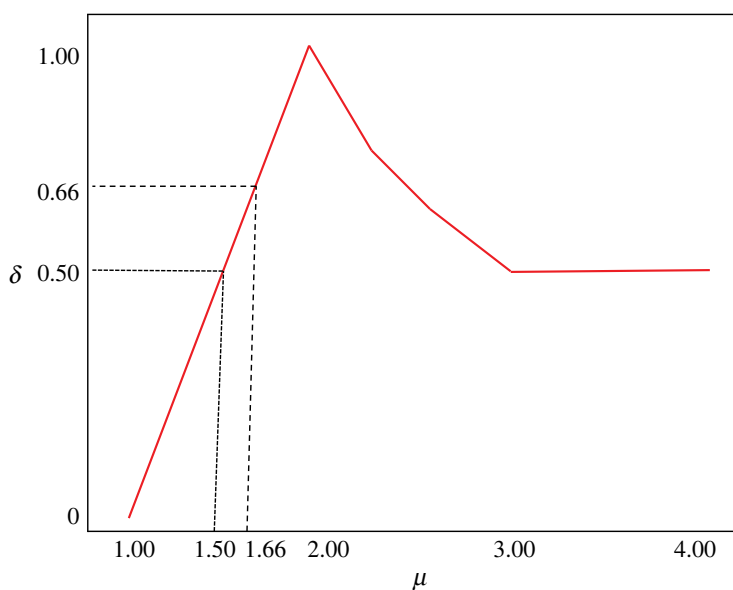


Figure 3. A plot of the relationship between the scaling index δ and the CE IPL index detected by using MDEA, with $\mu = \mu_S$. Note that $\delta = 0.5$ can also occur for $\mu_S = 1.5$ and $\mu_S \geq 3$. From Grigolini *et al.* [36] with permission.

with the MoS to detect information regarding the phenomenon of opinion persistence. It is well known that a diffusion trajectory generated by totally random fluctuations yields a rare recursion to the origin, with the time interval between consecutive origin crossings described by the hyperbolic PDF given by equation (1.1) with $\mu = 1.5$ [16]. Due to the forward stepping constraint on the RW in MDEA, we have: $\delta = \mu_S - 1$ for $1 < \mu_S < 2$ and $\delta = 1/(\mu_S - 1)$ for $2 < \mu_S < 3$, as well as $\delta = 0.5$ for $\mu_S \geq 3$ [35], as shown in figure 3.

Notice that the value $\delta = 0.66$ is the maximum scaling value occurring at $N = 150$. In the MDEA approach adopted herein, this scaling value signals the occurrence of the Kardar–Parisi–Zhang scaling [37]. According to the rule depicted by the solid black curve in figure 3, the scaling index

$\delta = 0.5$ is generated by the temporal complexity IPL index $\mu_S = 1.5$ for $\mu_S < 2$ and for all $\mu_S \geq 3$. The second condition is equivalent to an ordinary Poisson process. In summary, $\delta = 0.5$ may be determined by both CEs (with $\mu_S = 1.5$) and non-CEs (when $\mu_S \geq 3$).

Note that the heterogeneity observed in the many phenomena modelled by network theory are determined to be a consequence of the criticality of the underlying network dynamics. This perspective is non-reductionist, which is to say that the detailed behaviour of the individual elements no longer determines the behaviour of the network. Instead, the network or group behaviour is determined by an emergent property of the network dynamics, namely the average mean field behaviour. Near the critical point, the connectivity of the network elements is IPL in nature, and it is this IPL variability that provides for the network's necessary adaptability. Otherwise, a network might respond too strongly to the slightest perturbation, or be too indifferent and unresponsive to prolonged stimulation. The capacity of the mean field of a DMM network to produce the signal can be calculated in two different ways. One is to have every individual interact with every other individual on the lattice (all-to-all (ATA) coupling); the other is to have only the nearest neighbours interacting on a two-dimensional lattice with periodic boundary conditions. In practice, both calculations have critical values for a control parameter and critical dynamics, resulting in a graph of the non-monotonic behaviour of the scaling parameter δ as a function of N that essentially overlap one another. Thus, the response of the mean fields of differently configured networks to the same perturbation turns out to be similar.

The time interval between consecutive origin crossings provides information about the system maintaining its state, while MDEA applied to $\xi(t)$ detects the IPL index of CEs. Therefore, it is convenient to use the symbol μ_R to denote the complexity of the opinion-persistence (recrossing) index and the symbol μ_S to denote the index for the temporal complexity of CEs. When $N \neq 150$, but where the temporal complexity index is $\mu_S = 1.5$, we expect from equation (2.5) that the complexity opinion-persistence index will be $\mu_R = 1.75$. To evaluate μ_R , we study the diffusional variable $X(t)$, which will typically spend an extended time in the region $X(t) > 0$ (corresponding to the system selecting the 'yes' state) or an extended time in the region where $X(t) < 0$ (corresponding to the system selecting the 'no' state). This is the opinion-persistence effect, previously mentioned. Evaluating the IPL index μ_R is a challenging computational problem, but we can overcome this by applying the MDEA to $X(t)$. In this case, the scaling index δ evaluated by MDEA yields $\mu_R = 2 - \delta/2$. This scaling of δ is different from the scaling obtained by observing $\xi(t)$ directly, but the value of μ_R should be identical to the observation of the regression to the origin of $X(t)$, as we discuss in respect of the comparison of the calculated value with the empirically observed value in figure 6. Note that we used no prescribed time to run the diffusion calculation: the run must simply be long enough to obtain good statistics on the slope of the curve depicted in figure 2. This is typically equivalent to one and a half to two decades in model time covering the temporal complexity.

(d) Relations among scaling indices

The MDEA applied to empirical time series $\xi(t)$ determines the IPL index μ_S for the time-interval PDF for the transitions between the positive (negative) to negative (positive) values of $\xi(t)$. However, when applied to the generated diffusion process, $X(t)$ determines the IPL index μ_R for the time-interval PDF for the transitions between the positive (negative) to negative (positive) values of $X(t)$. A relation exists between these two scaling indices that is a consequence of the scaling property of the PDF for the diffusive trajectory

$$p(x, t) = \frac{1}{t^\delta} F\left(\frac{x}{t^\delta}\right). \quad (2.8)$$

Assuming that all the trajectories of a Gibbs system are located on the origin $X(0) = 0$ at $t = 0$, we have

$$p(0, t) = \sum_{n=1}^N \psi_n^{(R)}(t) = \frac{1}{t^\delta} F(0), \quad (2.9)$$

Table 1. Number of runs of SIM analysis for different principal network sizes (number of agents).

network size	no. simulations	network size	no. simulations
5	10	120	18
10	20	130	3
15	22	130	3
20	17	150	28
30	6	180	18
40	10	260	4
50	13	330	12
60	15	380	13
70	12	500	12
80	14	600	10
90	10	820	6
100	14	1000	3

For intermediate network sizes between these numbers, $N = 10$ in all cases.

where $\psi_n^{(R)}(t)$ is the probability that a trajectory starting from the origin at time $t = 0$ returns to the origin n times, with the last return occurring at time t . It is well known that if the recrossing of the origin is a renewal process, then it is readily determined that $\mu_R = 2 - \delta$. Using a continuous time random walk (CTRW), Failla *et al.* [38] established the relationship $\delta = (\mu_S - 1)/2$, thereby establishing a connection between μ_R and μ_S

$$\mu_R = 2 - \frac{\mu_S - 1}{2}, \quad (2.10)$$

a relation proposed by Failla & Grigolini [39] to account for the results obtained from the Barabási Ballistic Deposition model [40].

3. Results

Since the DMM and SIM models produce virtually identical results (see also the study of West *et al.* [16]), we here give results for the SIM analysis only. For the SIM analysis, we hold the noise parameter (denoted as η in Vicsek *et al.* [18]) constant at 1.35. Agent density (the other free parameter in the model of Vicsek *et al.* [18]) was adjusted by holding the simulation area constant and changing the number of agents (referred to as the ‘number of units’ in the figures), using a two-dimensional model so that density is equivalent to the number of agents per unit area. The analysis was run across a specified set of network sizes (range 5–1000 individuals), with an average of 12.6 (range 3–28) runs per network size (table 1). Since the principal focus for the analysis was on network sizes in the vicinity of the Dunbar layer sizes (5, 15, 50, 150 and 500), the number of runs is larger in the vicinity of these values. The values used to seed the runs were selected so as to be roughly evenly spaced on a log scale on either side of the prospective maxima corresponding to each Dunbar number (except in the case of $N = 5$ where networks less than five were meaningless). Smaller numbers of runs were carried out for intermediate values to provide an indication of the overall pattern.

Using the MoS, we record the times at which the fluctuations $\xi(t)$ cross the border between two consecutive stripes. Should these events not be crucial, they would not contribute to the scaling emerging in the long-time limit. Furthermore, when an event occurs, the random walker always makes a step ahead of constant intensity (length). Where the time series (t), with positive and negative fluctuations, is generated by CEs only, we obtain a CTRW [36], along with the scaling,

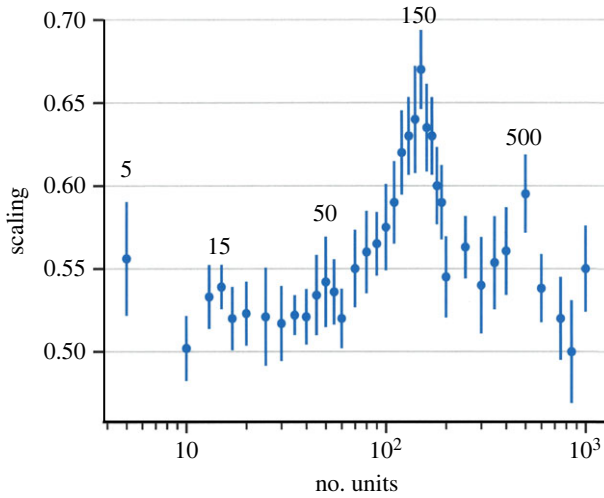


Figure 4. The scaling index δ shows its non-monotonic dependence on a network of size N using the SIM. Note the global maximum at the Dunbar Number 150 and the weaker secondary maximum at $N = 500$ and weaker still tertiary maxima at $N = 15$ and 50, commensurate with the layering of the Dunbar network. Symbols indicate means; error bars are standard deviations.

which can be properly evaluated using DEA without stripes: $\delta = (\mu_S - 1)/2$. In this case, the IPL index for CEs is given by $\mu_R = 2 - \delta$. Under the strict condition that both CEs and opinion persistence are renewal processes we obtain, using the relation between the scaling index δ and IPL index μ_R

$$\mu_R = 2 - \frac{\mu_S - 1}{2} = \frac{5 - \mu_S}{2}, \quad (3.1)$$

a relation originally proposed by Failla *et al.* [38] for studying the random growth of surfaces. Note that, since these results were obtained using the MDEA, this means that the fluctuation function $\xi(t)$ of SIM is not directly used to define the CEs.

We follow West *et al.* [16] and evaluate first the mean field for a SIM network to produce a signal. The calculations yield criticality at values of the scaling parameter whose local maxima depend on the size of the network. Identifying the calculated value of the time rate of change of the mean field variable with the empirical time series $\xi(t)$, we generate the RW and obtain the trajectory $X(t)$ to which we apply the MDEA to obtain the scaling index δ as a function of network size N (as detailed in §2). The resulting scaling parameter varies non-monotonically with the size of the network (figure 4).

In order to identify peaks in the distribution of δ -values in figure 4, polynomials of order 2–15 were fitted to the data. To avoid overfitting, we ran this analysis for $N \geq 10$ since in the natural world networks of five are superdense with very different structural characteristics. Figure 5 plots the goodness-of-fit (indexed by conventional r^2) as a function of equation order. Goodness-of-fit will always increase as more terms are added to the regression equation; instead, we seek the polynomial that optimizes fit. Although there are no formal methods for identifying the best-fit value in these cases, a convention is to identify the value on the X-axis equivalent to the point at which the slope changes (the point of diminishing returns). On an asymptotic graph, this can be identified as the value equivalent to the point on the Y-axis that is $1/e$ th down from the asymptote. This criterion identifies a ninth-order polynomial as the best-fit to the data ($r^2 = 0.348$, $t_{278} = 12.18$, $p < 0.0001$), suggesting that there are four peaks in the data between $10 \leq N \leq 1000$. Besides achieving a global maximum $\delta = \delta_m \approx 0.67$ when N is at the Dunbar number 150, the scaling index δ has additional local maxima with $\delta_m > \delta > 0.5$ at network sizes of $N \approx 15, 50$ and 500. Note how the data appear to be rising towards another peak at some value of $N > 1000$.

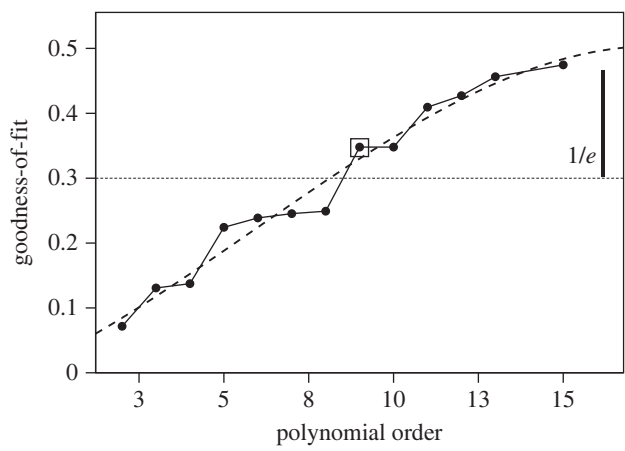


Figure 5. Goodness-of-fit (r^2) for different polynomial regression fits. The long-dashed line indicates the best-fit cubic regression fitted to these data. Note that goodness-of-fit approaches an asymptotic value at polynomials above the 13th order. The horizontal dotted line identifies the theoretical inflection point where the slope changes to yield diminishing returns (indexed as the value on the y-axis that is $1/e$ th down from the asymptote (indicated by a thick vertical line). The optimum polynomial order is a ninth-order equation (indicated by the boxed datapoint), with $r^2 = 0.348$ ($t_{278} = 12.18$, $p < 0.0001$). This also represents the largest absolute pairwise increase in goodness-of-fit.

Table 2. Comparison of δ -values in the vicinity of the predicted values network sizes of 15, 50, 150 and 500.

network sizes	t	d.f. ^b	p^c
peak versus comparison ^a			
5 versus 10	−2.15	18	0.0226
15 versus (10 + 20)	−51.87	52	<0.0001
50 versus (40 + 60)	−1.51	33	0.0600
150 versus (130 + 180)	−7.08	43	<0.0001
500 versus (380 + 600)	−4.12	26	0.0002

^aNumbers refer to those in table 1.
^bDue to correction for unequal variances, d.f. is less than the conventional $N-2$.
^cOne-tailed tests that the δ -values are higher on the peak than at the network sizes on either side (given in brackets in column 1).

Based on the observed layering in the empirical data on human group sizes [1], we would expect a further peak at around $N = 1500$. In effect, these inner and outer optima appear to be harmonics of the central peak at 150 (Dunbar’s number).

To confirm that the δ -values at network sizes of $N = 5, 15, 50, 150$ and 500 are indeed local maxima, we tested whether the values of δ at each of these maxima is higher than the values immediately on either side of them (or immediately to the right in the case of $N = 5$). The differences in each case are statistically significant or very close to significance (table 2). Taken together as a set, the peaks are significantly higher than the valleys between them (Fisher’s meta-analysis: $\chi^2 = 67.05$, d.f. = $2 \times 5 = 10$, $p < 0.0001$), indicating a consistent pattern across the five natural layer sizes.

We cannot emphasize too strongly that the peaks in figure 4 are determined only by the dynamic properties of the complex network, in the same way the single peak at the Dunbar Number was determined in the study of West *et al.* [16]. It is the critical nature of the network dynamics that determines the N -dependence of the scaling parameter δ . However, it is the

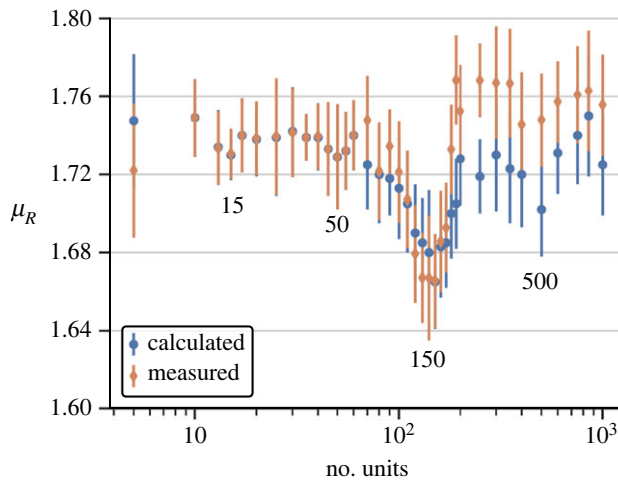


Figure 6. The theoretical IPL index for CEs is given in terms of the scaling index by equation (2.1) (red points). The experimental IPL index is calculated using MDEA to process $X(t)$ (blue points). Symbols indicate means; error bars are standard deviations.

emergent property of the network that determines the macroscopic behaviour; consequently, the dynamic behaviours of differently configured networks are inconsequential.

Of course, just as predicting the Dunbar Number alone did not establish that this network size optimizes the transmission of information between networks but required a separate calculation, the same is true for the other local maxima. This independent determination of the existence and location of layering numbers as a function of network size is made using the IPL scaling index (see West *et al.* [16]). The recrossing IPL index μ_R is determined by direct calculation from the diffusion trajectory and is compared with the theoretical values determined by the scaling parameter δ depicted in figure 4. The set of blue dots in figure 6 is obtained assuming the theoretical relation given by equation (3.1) is true and the scaling index δ has the values depicted in figure 4. In this case, the optima are indicated by the minima on the graph. It is evident that, despite modest divergence on the extremes of the graph, the fit is excellent (comparing means: Pearson $r = 0.709$, $N = 37$, $p < 0.0001$).

4. Discussion

A substantial number of observational studies [1–8] support the concept of Dunbar layering in human social networks. Independently of the mode of communication in human networks, the numerical values of the layered structure are remarkably consistent [1,3,41]. The present results suggest that the distinctive sizes of these layers (as observed in the empirical data) are the product of self-organizing processes in social networks that yield optimal information flow at networks of these specific values. The dependence of the scaling index on network size in figure 4 is one signature of complexity, and calculations in the study of West *et al.* [16] present a theory-predicted value for the optimal group size for humans that agrees with the empirical Dunbar number [1]. The theory also establishes that networks of this size have optimal information transmission properties in agreement with the PCM [18]. These values, thus, act as attractors both for network size and for the internal subnetwork structuring within these networks. It is of particular significance that these constraints on grouping size apply not just to humans [1] but also to the sizes and sub-structuring of anthropoid primate social groups as well as those of other mammals with complex multi-level social systems (e.g. elephants and orcas) [10–13,42].

The correspondence between theory and experiment (computation) in figure 6 is clearly excellent, especially within the range $10 \leq N \leq 200$, after which there is a 3–4% deviation between

the two, with a somewhat larger deviation at the lower end ($N=5$). However, a difference of even this magnitude cannot be considered large and we may be requiring too much from the computation, given the simplicity of the SIM model, to expect the fit to be exact. Notwithstanding this quantitative divergence, the two sequences are highly correlated: in figure 6, we observe the same qualitative dipping of the two curves in the vicinity of $N=500$, with weaker dips in the vicinity of $N=5$, 15 and $N=50$.

A secondary feature of the structure of these networks is the consistency of the scaling parameter, with its distinctive scaling ratio of approximately 3 across layers [1]. The strength of the scaling parameter in actual social networks does not vary with the layer size, but is remarkably consistent [1]. This was investigated by Mac Carron *et al.* [5] using a very large mobile phone dataset to determine whether the layering can be identified based on call frequency alone. Using several different statistical methods, they found that the interaction frequencies clustered in a way that consistently yielded the Dunbar layers. This sensitivity of the layering structure to the size of the population is given further support by the change in the coupling of the elements of the DMM network in our theoretical model [16]: comparing the dependence of the scaling index δ on the size of the network N for a square lattice with nearest neighbour only interactions with that for an ATA coupling of the elements on the lattice produced nearly identical results (fig. 1 in West *et al.* [16]).

Mac Carron *et al.* [5] were unable to provide an explanation as to why these structured layers should have such a consistent pattern. The present findings go some way towards providing an explanation: the efficiency with which information flows around the network is optimized at these particular network values. There are two alternative ways this might come about. One is that when large groups are created (presumably in response to some external selection pressure), a natural top-down sub-structuring of the internal network takes place into a set of distinct sub-networks that each represent local optima, producing a top-down cascade of sub-structuring to yield the layers we observe. Alternatively, large groups may be produced, when required by some external need, by a bottom-up process of agglutination whereby sets of lower level groupings are 'bolted' together to create a higher level grouping (three 15-layer groups create a 50-layer, three 50-layer groups create a 150-layer, etc.). If the base unit is always of a constant size in all species (as appears to be the case [27]), this would explain why only certain group sizes are possible [10]. What remains to be explained is why the scaling relationship is approximately 3, rather than, say, approximately 2 or approximately 4. This may have something to do with the dynamic stability of social triads [43] and the way these are held together by time-dependent bonded relationships [44].

In real-life networks, it seems that the layers in human networks, at least, are related to emotional rather than cognitive closeness [35,45,46]. This is consistent with the two-system model of the brain proposed by Kahneman [47], in which System 1 (intuition) has a fast, almost immediate response time and System 2 (cognition) has a much slower response time due to the need to organize logical thinking. It seems likely that the fast-acting intuitive part of the brain is primarily responsible for the layering structure, in support of the emotional rather than cognitive closeness of the individuals within the group [44], as discussed at length by West *et al.* [33]. The fact that the cognitive component converges on the same solution, albeit more slowly, is supported by the finding that the layers emerge naturally out of a first principles model of optimal decisions on how social capital should be invested in different alters when the benefits they offer differ in value [39,48,49].

In sum, it appears that Dunbar layering is a consequence of the nonlinear dynamics of the underlying complexity of networks that set up a series of fractally patterned attractors for group size as a consequence of efficiencies in information flow. The critical nature of the dynamics gives rise to a size dependence of the interaction parameter thereby entailing a size dependence on the parameter value at which criticality occurs. One way this might arise is that it is the effectiveness with which the smallest groupings are integrated that percolates through to determine the efficiency of the 150 groupings: a set of well-ordered 15-groupings necessarily creates a well-ordered 150-grouping. These results have obvious implications for our

understanding of pathogen transmission, as well as the way in which social media and online multi-player gaming environments are organized [3,8,50]. It has been suggested that several physical and chemical properties due to the thermodynamics of finite-sized systems, including protein folding [51] and the chain length dependence of the optical properties of Perovskites [52], may analogously be due to such collective behaviour.

Data accessibility. The computer code can be found from the Github repository: <https://github.com/garland-culbreth/Diffusion-Entropy-Analysis>.

Authors' contributions. B.J.W.: conceptualization, formal analysis, methodology, supervision, writing—original draft and writing—review and editing; R.I.M.D.: conceptualization, formal analysis, writing—original draft and writing—review and editing; G.C.: formal analysis, investigation, methodology and writing—review and editing; P.G.: conceptualization, methodology, supervision, validation and writing—review and editing.

All authors gave final approval for publication and agreed to be held accountable for the work performed therein.

Conflict of interest declaration. We declare we have no competing interests.

Funding. We received no funding for this study.

References

1. Dunbar RIM. 2020 Structure and function in human and primate social networks: implications for diffusion, network stability and health. *Proc. R. Soc. A* **476**, 20200446. (doi:10.1098/rspa.2020.0446)
2. Zhou WX, Sornette D, Hill RA, Dunbar RIM. 2005 Discrete hierarchical organization of social group sizes. *Proc. Biol. Sci. B* **272**, 439–444. (doi:10.1098/rspb.2004.2970)
3. Dunbar RIM, Arnaboldi V, Conti M, Passarella A. 2015 The structure of online social networks mirrors those in the offline world. *Soc. Netw.* **43**, 39–47. (doi:10.1016/j.socnet.2015.04.005)
4. Wang P, Ma JC, Jiang ZQ, Zhou WX, Sornette D. 2020 Comparative analysis of layered structures in empirical investor networks and cellphone communication networks. *EPJ Data Sci.* **9**, 11. (doi:10.1140/epjds/s13688-020-00230-1)
5. Mac Carron P, Kaski K, Dunbar RIM. 2016 Calling Dunbar's numbers. *Soc. Netw.* **47**, 151–155. (doi:10.1016/j.socnet.2016.06.003)
6. Hamilton MJ, Milne BT, Walker RS, Burger O, Brown JH. 2007 The complex structure of hunter-gatherer social networks. *Proc. R. Soc. B* **274**, 2195–2202. (doi:10.1098/rspb.2007.0564)
7. Kordsmeyer T, Mac Carron P, Dunbar RIM. 2017 Sizes of permanent campsites reflect constraints on natural human communities. *Curr. Anthropol.* **58**, 289–294. (doi:10.1086/690731)
8. Fuchs B, Sornette D, Thurner S. 2014 Fractal multi-level organization of human groups in a virtual world. *Sci. Rep.* **4**, 6526. (doi:10.1038/srep06526)
9. Dunbar RIM. 2011 Constraints on the evolution of social institutions and their implications for information flow. *J. Inst. Econ.* **7**, 345–371. (doi:10.1017/S1744137410000366)
10. Dunbar RIM, Mac Carron P, Shultz S. 2018 Primate social group sizes exhibit a regular scaling pattern with natural attractors. *Biol. Lett.* **14**, 20170490. (doi:10.1098/rsbl.2017.0490)
11. Hill RA, Bentley A, Dunbar RIM. 2008 Network scaling reveals consistent fractal pattern in hierarchical mammalian societies. *Biol. Lett.* **4**, 748–751. (doi:10.1098/rsbl.2008.0393)
12. Escribano D, Doldán-Martelli V, Cronin KA, Haun DB, van Leeuwen EJ, Cuesta JA, Sánchez A. 2022 Chimpanzees organize their social relationships like humans. *Sci. Rep.* **12**, 16641. (doi:10.1038/s41598-022-20672-z)
13. Dunbar RIM, Shultz S. 2021 Social complexity and the fractal structure of social groups in primate social evolution. *Biol. Rev.* **96**, 1889–1906. (doi:10.1111/brv.12730)
14. Shultz S, Dunbar RIM. 2022 Socioecological complexity in primate groups and its cognitive correlates. *Phil. Trans. R. Soc. B* **377**, 20210296. (doi:10.1098/rstb.2021.0296)
15. Shultz S, Noe R, McGraw S, Dunbar RIM. 2004 A community-level evaluation of the impact of prey behavioral and ecological characteristics on predator diet composition. *Proc. R. Soc. Lond. B* **271**, 725–732. (doi:10.1098/rspb.2003.2626)
16. West BJ, Massari GF, Culbreth G, Failla R, Bologna M, Dunbar RIM, Grigolini P. 2020 Relating size and functionality in human social networks through complexity. *Proc. Natl Acad. Sci. USA* **117**, 18 355–18 358. (doi:10.1073/pnas.2006875117)
17. West BJ, Turluska M, Grigolini P. 2014 *Networks of echoes: imitation, innovation and invisible leaders*. New York, NY: Springer.

18. Vicsek T, Czirkok A, Ben-Jacob E, Cohen I, Shochet O. 1995 Novel type of phase transition in a system of self-driven particles. *Phys. Rev. Lett.* **75**, 1226–1231. (doi:10.1103/PhysRevLett.75.1226)
19. Lorenz J. 2007 Continuous opinion dynamics under bounded confidence: a survey. *Int. J. Mod. Phys. C* **18**, 1819–1838. (doi:10.1142/S0129183107011789)
20. Waagen A, Verma G, Chan K, Swami A, D'Souza R. 2015 Effect of zealotry in high-dimensional opinion dynamics models. *Phys. Rev. E* **91**, 022811. (doi:10.1103/PhysRevE.91.022811)
21. Peralta AF, Kertész J, Iñiguez G. 2022 Opinion dynamics in social networks: from models to data. (<https://arxiv.2201.01322>)
22. West BJ, Geneston EL, Grigolini P. 2008 Maximizing information exchange between complex networks. *Phys. Rep.* **468**, 1–99. (doi:10.1016/j.physrep.2008.06.003)
23. Barenblatt GI. 1996 *Scaling, self-similarity and intermediate asymptotics*. Cambridge, UK: Cambridge University Press.
24. Abney DH, Paxton A, Dale R, Kello CT. 2014 Complexity matching in dyadic conversation. *J. Exp. Psychol.* **143**, 2304–2315. (doi:10.1037/xge0000021)
25. Almurad ZMH, Roume C, Blain H, Delignières D. 2018 Complexity matching: restoring the complexity of locomotion in older people through arm-in-arm walking. *Front. Physiol.* **9**, 1766. (doi:10.3389/fphys.2018.01766)
26. Wiener N. 1948 Time, communication and the nervous system. *Proc. NY Acad. Sci.* **50**, 197–220. (doi:10.1111/j.1749-6632.1948.tb39853.x)
27. Dunbar RIM. 2023 Structural and cognitive solutions to prevent group fragmentation in group-living species. *bioRxiv*. (doi:10.1101/2022.12.13.520310)
28. Dunbar RIM. 2022 Virtual touch and the human social world. *Curr. Opin. Behav. Sci.* **43**, 14–19. (doi:10.1016/j.cobeha.2021.06.009)
29. Stanley HE, Buldyrev SV, Goldberger AL, Goldberger ZD, Havlin S, Mantegna RN, Ossadnik SM, Peng CK, Simons M. 1994 Statistical mechanics in biology: how ubiquitous are long-range correlations? *Phys. A* **205**, 214. (doi:10.1016/0378-4371(94)90502-9)
30. Peng CK, Buldyrev SV, Havlin S, Simons M, Stanley HE, Goldberger AL. 1994 Mosaic organization of DNA nucleotides. *Phys. Rev. E* **49**, 1685. (doi:10.1103/PhysRevE.49.1685)
31. Couzin J. 2007 Collective minds. *Nature* **445**, 715. (doi:10.1038/445715a)
32. Culbreth G, West BJ, Grigolini P. 2019 Entropic approach to the detection of crucial events. *Entropy* **21**, 178. (doi:10.3390/e21020178)
33. West BJ, Mahmoodi K, Grigolini P. 2019 *Empirical paradox, complexity thinking and generating new kinds of knowledge*. Newcastle, UK: Cambridge Scholars Publishing.
34. Mandelbrot BB, van Ness JW. 1968 Fractional Brownian motions, fractional noises and applications. *SIAM Rev.* **10**, 422. (doi:10.1137/1010093)
35. Redner S. 2001 *A guide to first-passage processes*. Cambridge, UK: Cambridge University Press.
36. Grigolini P, Palatella L, Raffaelli G. 2001 Asymmetrical anomalous diffusion: an efficient way to detect memory in time series. *Fractals* **9**, 439. (doi:10.1142/S0218348X01000865)
37. Weiss GH. 1994 *Aspects and applications of the random walk*. Amsterdam, The Netherlands: North Holland Press.
38. Failla R, Grigolini P, Ignaccolo M, Schwettmann A. 2004 Random growth of interfaces as a subordinated process. *Phys. Rev. E* **70**, 010101. (doi:10.1103/PhysRevE.70.010101)
39. Failla R, Grigolini P. 2005 The search for crucial events, visible or invisible, as a physical road to subordination. *Fluct. Noise Lett.* **5**, L175. (doi:10.1142/S0219477505002537)
40. Barabási AL. 1995 *Fractal concepts in surface growth*. Cambridge, UK: Cambridge University Press.
41. Arnaboldi V, Conti M, Passarella A, Dunbar RIM. 2017 Online social networks and information diffusion: the role of ego networks. *Online Soc. Netw. Media* **1**, 44–55. (doi:10.1016/j.osnem.2017.04.001)
42. Kudo H, Dunbar RIM. 2001 Neocortex size and social network size in primates. *Anim. Behav.* **62**, 711–722. (doi:10.1006/anbe.2001.1808)
43. Cartwright D, Harary F. 1956 Structural balance: a generalization of Heider's theory. *Psychol. Rev.* **63**, 277–292. (doi:10.1037/h0046049)
44. Dunbar RIM. 2018 The anatomy of friendship. *Trends Cogn. Sci.* **22**, 32–51. (doi:10.1016/j.tics.2017.10.004)
45. Sutcliffe AG, Dunbar RIM, Binder J, Arrow H. 2012 Relationships and the social brain: integrating psychological and evolutionary perspectives. *Br. J. Psychol.* **103**, 149–168. (doi:10.1111/j.2044-8295.2011.02061.x)

46. Sutcliffe AG, Binder J, Dunbar RIM. 2018 Activity in social media and intimacy in social relationships. *Comp. Hum. Beha.* **85**, 227–235. (doi:10.1016/j.chb.2018.03.050)
47. Kahneman D. 2011 *Thinking, fast and slow*. Farrar, Italy: Straus and Grioux.
48. Tamarit I, Cuesta J, Dunbar RIM, Sánchez A. 2018 Cognitive resource allocation determines the organisation of personal networks. *Proc. Natl Acad. Sci. USA* **115**, 1719233115. (doi:10.1073/pnas.1719233115)
49. Tamarit I, Sánchez A, Cuesta JA. 2022 Beyond Dunbar circles: a continuous description of social relationships and resource allocation. *Sci. Rep.* **12**, 2287. (doi:10.1038/s41598-022-06066-1)
50. Dunbar RIM. 2016 Do online social media cut through the constraints that limit the size of offline social networks? *R. Soc. Open Sci.* **3**, 150292. (doi:10.1098/rsos.150292)
51. Bereau T, Bachmann M, Desemo M. 2010 Interplay between secondary and tertiary structure formation in protein folding cooperativity. *J. Am. Chem. Soc.* **132**, 13 129–13 131. (doi:10.1021/ja105206w)
52. Nagasaka H, Yoshizawa-Fujita M, Takeoka Y, Rikukawa M. 2018 Tuning the structures and optical properties of perovskites by varying the alkylamine type and chain length. *ACS Omega* **3**, 1892. (doi:10.1021/acsomega.8b02399)